Stochastic analysis of the power systems excited by fractional Gaussian noise

Shaojuan Ma(马少娟), Hufei Li(李虎飞), Bin Pei(裴斌), Yong Xu(许勇)

Citation: Chin. Phys. B. 35, 104501 (2026). DOI: 10.1088/1674-1056/ae1fe8 | CSTR: 32038.14.CPB.ae1fe8
http://cpb.iphy.ac.cn; http://iopscience.iop.org/cpb

What follows is a list of articles you may be interested in

Resistance law of a rod penetrating a multilayer granular raft

Zonglin Li(李宗霖), Qiang Tian(田强), Haiyan Hu(胡海岩)
Chin. Phys. B. 32, 034501 (2023). DOI: 10.1088/1674-1056/aca5ff

Inhibitory effect induced by fractional Gaussian noise in neuronal system

Zhi-Kun Li(李智坤), Dong-Xi Li(李东喜)
Chin. Phys. B. 32, 010203 (2023). DOI: 10.1088/1674-1056/ac6332

Practical security analysis of continuous-variable quantum key distribution with an unbalanced heterodyne detector

Lingzhi Kong(孔令志), Weiqi Liu(刘维琪), Fan Jing(荆凡), Chen He(贺晨)
Chin. Phys. B. 31, 070303 (2022). DOI: 10.1088/1674-1056/ac4102

Most probable transition paths in eutrophicated lake ecosystem under Gaussian whit e noise and periodic force

Jinlian Jiang(姜金连), Wei Xu(徐伟), Ping Han(韩平), Lizhi Niu(牛立志)
Chin. Phys. B. 31, 060203 (2022). DOI: 10.1088/1674-1056/ac5616

Stochastic analysis of the power systems excited by fractional Gaussian noise

Shaojuan Ma(马少娟)[1], Hufei Li(李虎飞)[1], Bin Pei(裴斌)[2,3,†], and Yong Xu(许勇)[2]

[1] *School of Mathematics and Information Science and Ningxia Key Laboratory of Intelligent Information and Big Data Processing, North Minzu University, Yinchuan* 750021, *China*

[2] *School of Mathematics and Statistics and MOE (Ministry of Education) Key Laboratory for Complexity Science in Aerospace, Northwestern Polytechnical University, Xi'an* 710072, *China*

[3] *Research & Development Institute of Northwestern Polytechnical University in Shenzhen, Shenzhen* 518057, *China*

(Received 20 October 2025; revised manuscript received 6 November 2025; accepted manuscript online 17 November 2025)

This paper is devoted to studying the impacts of fractional Gaussian noise (FGN) excitation on power systems. Firstly, based on the historical data of power systems, the long-range correlations in power systems are found, and then the power systems under FGN excitation are established. Secondly, to quantify the influences of FGN on the proposed models, the security-domain probability is introduced. Thirdly, according to the pathwise integrals and differential rule with respect to FGN, an analytical method is proposed to evaluate the security-domain probability. In contrast to the Monte Carlo approach, the analytical approach is much faster to yield the security-domain probability without losing the accuracy of results. Finally, some suggestions are offered to enhance the dynamical characteristics of the FGN-excited power systems.

Keywords: fractional Gaussian noise, multi-generator power systems, energy function, security-domain probability

PACS: 45.10.Hj, 05.40.–a, 05.10.Gy

DOI: 10.1088/1674-1056/ae1fe8 **CSTR:** 32038.14.CPB.ae1fe8

1. Introduction

With the rising popularity of solar power generation, wind power generation, and other new energy sources, their randomness and uncertainty bring significant difficulties to the regulation and operation of power systems. The research on power systems under the influence of randomness and uncertainty has received much attention.[1–3] Thus, it is important to analyze the influence of uncertainty and randomness for stochastic differential equations (SDEs) modeling[4–6] in renewable power systems. Yuan *et al.*[7] considered wind power as a stochastic disturbance and developed dynamical power systems based on SDEs. Wang *et al.*[8] determined the effect of Gaussian white noise (GWN) perturbation on power system stability based on Fokker–Planck–Kolmogorov equations. Ghanavati *et al.*[9] modeled power systems subjected to stochastic load perturbations and different renewable energy generation as stochastic differential algebraic equations. Ju *et al.*[10] discussed the impact of an additive GWN on power system characteristics according to stochastic dynamical methods. Most of the research on the stochastic dynamics of power systems focuses on the case of Gaussian white noise excitation. Although a few studies have considered the influence of temporal correlation in random factors on the system characteristics, the research is not in-depth.[11]

However, the randomness of new energy output in reality has strong temporal correlations that memoryless noise models, *i.e.*, GWN, are often unable to adequately capture.[12,13] Fractional Brownian motion (FBM) provides an important theoretical basis for the investigation of long-correlation noise. It is a more extensive stochastic process than Brownian motion (BM). The parameter known as H in FBM $B^H(t)$ and fractional Gaussian noise (FGN) $W^H(t)$, which is the formal derivative of the FBM, is referred to as the Hurst index, a concept defined in the interval $0 < H < 1$. In the case of $H = 1/2$, the FBM $B^H(t)$ reduces to the standard BM $B(t)$, and the FGN $W^H(t)$ reduces to GWN $W(t)$. An FBM $B^H(t)$ with $H \neq 1/2$ is neither a semimartingale nor a Markov process. It is evident that the responses of systems to FGN cannot be treated as a Markov diffusion process, and the conventional Itô stochastic calculus cannot be applied. The calculus with respect to the FBM is intricate, and its mathematical theory is still in development.[14–16] Consequently, the investigation of nonlinear dynamical systems excited by FGN presents significant difficulties and challenges.

Summarily, in the modeling of the randomness of new energy power, the probabilistic distribution properties and the time-correlation of different variables are required to be considered. Besides, the primary key problem is how to model the randomness of new energy power with its time-correlation and probabilistic distribution properties into power systems. De-

†Corresponding author. E-mail: binpei@nwpu.edu.cn

© 2026 Chinese Physical Society and IOP Publishing Ltd. All rights, including for text and data mining, AI training, and similar technologies, are reserved.

spite the employment of various noise models to describe random perturbations in power systems, FGN provides distinct advantages for the modeling of realistic flight environments. Contrary to the assumption of independence between increments made by memory-less noise processes, FGN captures the long-range temporal correlations that are commonly observed in wind farms. Therefore, establishing an FGN model to accurately describe the randomness of new energy power with time-correlation and probabilistic distribution properties can both ensure the accuracy and incorporate the randomness of new energy power in a more efficient way. Thus, a new stochastic dynamical model for power systems excited by FGN is established in this paper. Then, the analytical approach based on pathwise integrals and the differential rule with respect to FGN has several key advantages over Monte Carlo simulation.[18] Firstly, it achieves superior computational efficiency by avoiding the large-scale, repeated sampling and fine time-stepping that are inherent in Monte Carlo simulation. This reduces computational time by orders of magnitude while maintaining accuracy. Furthermore, it enables deterministic error control by yielding closed-form expressions for key metrics, allowing for a more systematic assessment of accuracy without the sampling variance that plagues Monte Carlo simulation results. In addition to improving efficiency and precision, the method provides deeper parametric insight by establishing closed-form dependencies on critical parameters such as the Hurst index, noise intensity, and critical energy. This makes it possible to conduct direct sensitivity analysis, which would otherwise be difficult to obtain from Monte Carlo simulation alone.

The present work is organized as follows. In Section 2, a few preliminaries such as the FGN and the FBM are introduced. Section 3 proposes the model of power systems excited by FGN. Section 4 puts forward the analytical method for the dynamical effect of FGN excitation on the proposed systems. Section 5 offers simulation examples to illustrate the application and validity of this technique in power systems. Finally, Section 6 presents some conclusions.

2. Preliminaries

2.1. Long-range correlation in power systems

Based on the measured power data of wind farms and photovoltaic power plants in the same area,[17] the correlation between wind power generation (WPG) and photovoltaic power generation (PPG) is investigated by detrended fluctuation analysis (DFA). The generated wind and photovoltaic power generation curves are shown in Fig. 1. As seen from Fig. 1, wind and photovoltaic power generation have obvious seasonal periodicity. In addition, the power generation at a certain time in the future is not only related to the current power generation but also related to the power generation in the past.

For quantifying the correlation between the time series of wind and photovoltaic power generation, we use the DFA introduced by Peng *et al.*[19] This approach is suitable for quantifying the long-range correlation in non-stationary signals and has been successfully applied to weather records,[20,21] financial data,[22] and so on. The DFA process is briefly described below. The original time series $x(i)$, $i = 1,2,\ldots,N$ is integrated to yield $y(k) = \sum_{i=1}^{k}[x(i) - \langle x\rangle]$, $k = 1,\ldots,N$, where $\langle x\rangle = \frac{1}{N}\sum_{i=1}^{N} x(i)$ is the average. Then, the sequence $y(k)$ is divided into N_n non-overlapping segments with length n, and the linear least square fitting is estimated in each segment ($s = 1,2,\ldots,N_n$). Next, the trend of the sequence $y(k)$ is solved by subtracting the local trend from the data in each segment. The detrended variance can be calculated as

$$F^2_{\mathrm{DFA}}(n) = \frac{1}{nN_n}\sum_{s=1}^{N_n}\sum_{k=n(s-1)+1}^{ns}[y(k) - y_{n,s}(k)]^2, \tag{1}$$

where $F_{\mathrm{DFA}}(n)$ usually increases with n based on the power law $F_{\mathrm{DFA}}(n) \sim n^{\alpha}$. The scaling exponent α is the slope of least square fitting of $\log[F_{\mathrm{DFA}}(n)]$ with respect to $\log n$. When $\alpha = 0.5$ means uncorrelated signal, $\alpha > 0.5$ represents persistent long-range correlation and $\alpha < 0.5$ denotes anti long-distance correlation. The scaling exponent α corresponds to the Hurst index H in FGN.[23,24]

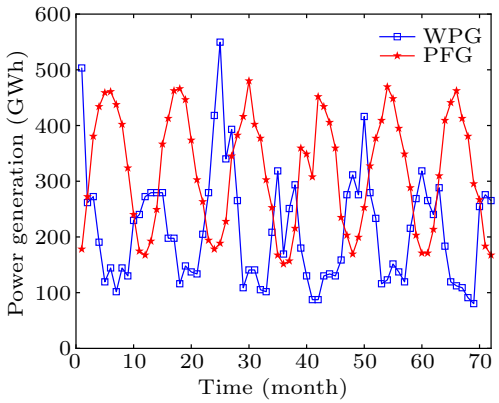

Fig. 1. The generated wind and photovoltaic power generation curves.

In order to verify the long-range correlation between wind and photovoltaic power generation data, we present the results of DFA1, DFA2, and DFA3 in Figs. 2 and 3. In Fig. 2, the scaling exponents under DFA of orders 1, 2, and 3 are respectively $\alpha_1 = 0.88 \pm 0.02, \alpha_2 = 0.83 \pm 0.01, \alpha_3 = 0.82 \pm 0.01$. In Fig. 3, the scaling exponents under DFA of orders 1, 2, and 3 are respectively $\alpha_1 = 0.69 \pm 0.01, \alpha_2 = 0.70 \pm 0.01, \alpha_3 = 0.71 \pm 0.01$. From Figs. 2 and 3, both wind and photovoltaic power generation dynamics exhibit persistent long-range correlation ($\alpha > 0.5$). Among them, the correlation of wind power generation is stronger, as shown by the higher value of the scaling exponent.

To sum up, it is necessary to consider the long-range correlation between different variables in the modeling of renewable power systems. Therefore, introducing FGN with long-range correlation into the power system model can not only ensure accuracy but also efficiently analyze the operation of renewable power systems.

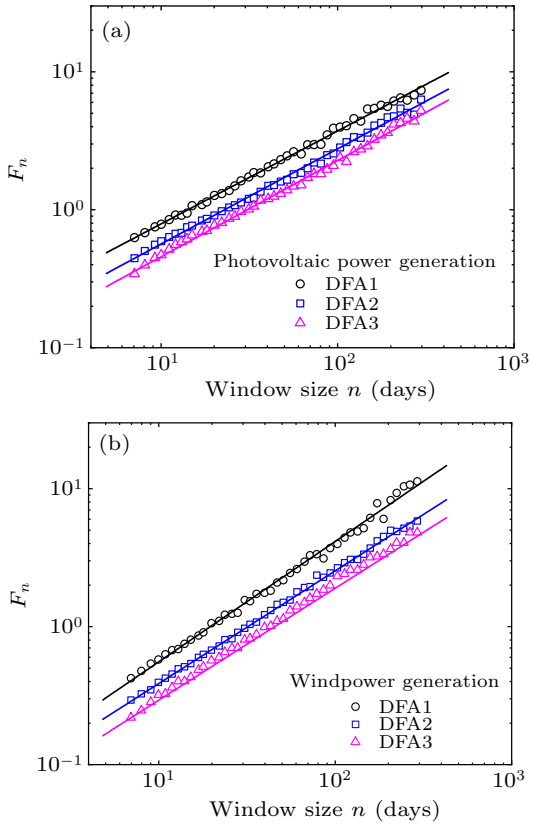

Fig. 2. The DFA of orders 1, 2, and 3: (a) daily wind power generation, (b) daily photovoltaic power generation.

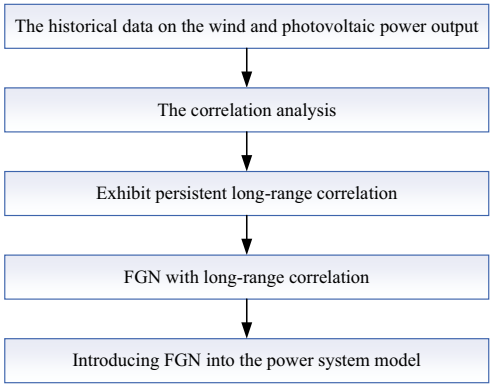

Fig. 3. The motivation of power system modeling under FGN excitation.

2.2. FBM and FGN

FBM was defined by Mandelbrot and Van Ness, who presented in Ref. [25] a random integration in the form of standard BM, *i.e.*

$$B^H(t) = C_H\left\{\int_{-\infty}^{0}[(t-s)^{H-1/2}-(-s)^{H-1/2}]\mathrm{d}B(s) + \int_0^t (t-s)^{H-1/2}\mathrm{d}B(s)\right\}, \tag{2}$$

in which $B(t)$ is a standard BM and C_H is a normalization constant.

Definition 1 Let the Hurst index be $H \in (0,1)$. FBM $(B^H(t))_{t\geq 0}$ is the continuous, centered Gaussian process whose covariance function is

$$\mathbb{E}[B^H(t)B^H(s)] = \frac{1}{2}(t^{2H}+s^{2H}-|t-s|^{2H}), \quad t,s\geq 0, \tag{3}$$

where $t,s\in\mathbb{R}_+$.

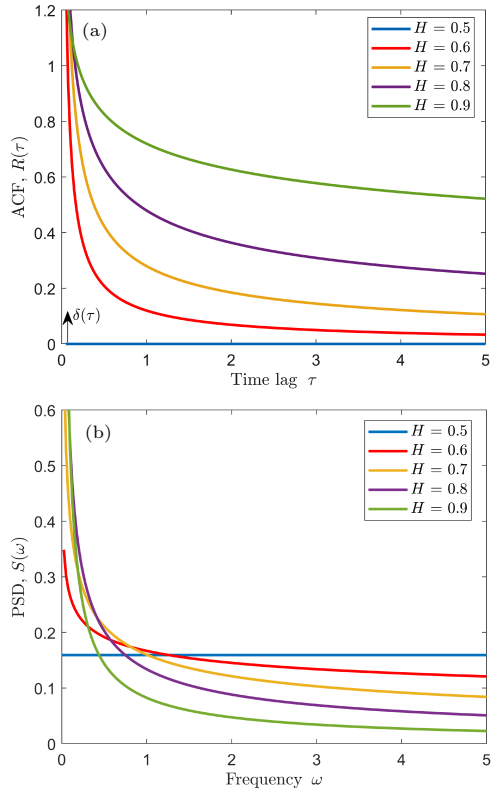

Fig. 4. ACF and PSD of FGN: (a) ACF, (b) PSD.

Suppose $H = 1/2$; FBM will then be the standard BM. Via Definition 1, when $H > 1/2$, the FBM process $(B^H(t), t \geq 0)$ exhibits a long-distance correlation. When $r(n) = \mathbb{E}[B^H(1)(B^H(n+1)-B^H(n))]$, thus $\sum_{n=1}^{\infty} r(n) = \infty$. The FBM likewise exhibits self-similarity; then $(B^H(\alpha t), t \geq 0)$ features the identical probability density law as $(\alpha^H B^H(t), t \geq 0)$. Similar to the standard BM, FBM is non-differentiable a.s. (almost surely). Since the formal derivative of BM is often called GWN, the FBM is called FGN, *i.e.*

$$W^H(t) = \frac{\mathrm{d}B^H(t)}{\mathrm{d}t} = \frac{B^H(t+\Delta t)-B^H(t)}{\Delta t}. \tag{4}$$

Then, according to Eqs. (3) and (4), the auto-correlation function (ACF) of FGN can be derived, *i.e.*

$$\begin{aligned} R(\tau) &= \mathbb{E}[W^H(t+\tau)W^H(t)] \\ &= H(H+1)|\tau|^{2H-2} + 2H|\tau|^{2H-1}\delta(\tau). \end{aligned} \tag{5}$$

This could easily indicate that $R(\tau)$ is the Dirac function $\delta(\tau)$ from Eq. (5) as $H = 1/2$, and it is the ACF of GWN. Using

Fourier transformation, the power spectral density (PSD) of FGN with $1/2 \le H < 1$ would be acquired as follows:

$$S(\omega) = \frac{1}{2\pi}\int_{-\infty}^{\infty} R(\tau)\,\mathrm{e}^{-\mathrm{j}\omega\tau}\,\mathrm{d}\tau = \frac{H\Gamma(2H)\sin(H\pi)}{\pi}|\omega|^{1-2H}. \tag{6}$$

Figure 4 displays a few simulation results with ACF and PSD of FGN when $1/2 \le H < 1$. According to Fig. 4, the PSD is close to a constant while the ACF approaches the Dirac function $\delta(\tau)$ as H approaches $1/2$. When H is close to 1, the PSD is close to the Dirac function $\delta(\tau)$ while the ACF is close to a constant. When H is between $1/2$ and 1, the ACF is limited to a value in a long time interval, which indicates long-range correlation. Thus, when H with $1/2$ and 1, FGN is a steady Gaussian process. Figure 5 provides an intuitive observation for FGN with different Hurst index H.

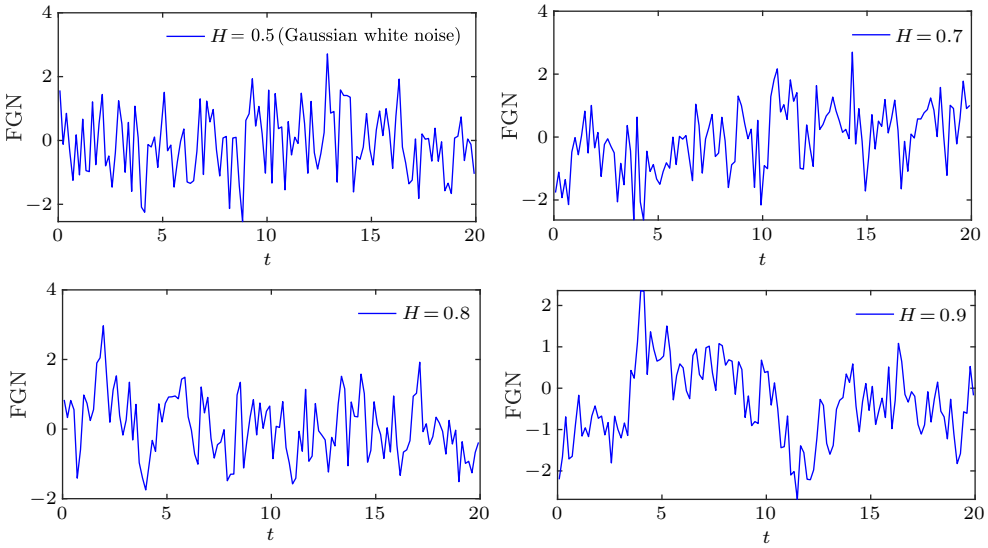

Fig. 5. The sample path of FGN for different Hurst indexes (a) $H = 0.5$, (b) $H = 0.7$, (c) $H = 0.8$, (d) $H = 0.9$.

3. Modeling

3.1. The model of power systems excited by FGN

In the environment of increasing integration among renewable energy generation and rechargeable vehicles, more and more uncertainty and randomness are brought into power systems. FGN is regarded as the random perturbation of the bus load power with long-range dependence. Thus, the multi-machine power systems excited by FGN are as follows:

$$\begin{cases} \mathrm{d}\delta_i = \omega_0\Delta\omega_i\,\mathrm{d}t \quad i = 1,2,\ldots,n, \\ M_i\,\mathrm{d}\Delta\omega_i = (P_i - P_{ei} - D_i\Delta\omega_i)\,\mathrm{d}t + \sigma_i\,\mathrm{d}B_i^{H_i}(t), \end{cases} \tag{7}$$

with

$$\begin{cases} P_i = P_{mi} - G_{ii}E_i^2, \\ P_{ei} = \sum_{j=1,j\neq i}^{n} E_iE_jB_{ij}\sin(\delta_i - \delta_j), \end{cases} \tag{8}$$

in which n is the number of generators, δ_i, $\Delta\omega_i$, M_i, E_i, and D_i are respectively the rotating angle, rotating rate, inertial parameter, generator energy, damping coefficient, and internal voltage of the i-th machine, and $\omega_0 = 2\pi f$ is the synchronous speed. $G_{ii}E_i^2$ represents the effective power generated by the loads, because the network and the load are combined. G_{ii} and B_{ij} are terms in the simplified mobility matrix. $\sigma_i\mathrm{d}B_i^H$ stands for the FGN excitation on the i-th generator, $B_i^{H_i}$ represents the independent FBM, H_i is the Hurst index in the range of $1/2 < H_i < 1$, and σ_i is the intensity of the FGN excitation in the i-th machine.

3.2. The security-domain probability

When the power systems are subject to deterministic disturbances, the smaller perturbations have a weaker impact. However, for power systems subjected to random perturbations, the small perturbations could have dramatic influences.[26] In practice, it is preferable that system states function in the secure region. Maintaining system frequency within specific limitations is necessary to achieve frequency performance standards.[10,27] When uncertain variability is added, system states within the area are determined at random. The likelihood of operational states occurring in an area is an appropriate metric for assessing the effects of unknown variability on power system characteristics. In this study, we refer to this probability as the security-domain probability. Stable power systems with greater security-domain probabilities may be less affected by unknown variability. The security-domain probability is then determined

$$\boldsymbol{P}(t) = \boldsymbol{P}\{Y(t) \in \Omega_{\mathrm{B}}\}, \tag{9}$$

where $Y(t)$ stands for running status such that

$$Y(t) = [\delta_1(t),\ldots,\delta_n(t),\Delta\omega_1,\ldots,\Delta\omega_n],$$

and $\Omega_{\rm B}$ indicates the secure domain required by the running status and $\boldsymbol{P}\{Y(t)\in\Omega_{\rm B}\}$ expresses the probability when $Y(t)$ lies in $\Omega_{\rm B}$.

3.3. Energy function for multi-generator power systems

For single-generator-infinite-bus power systems with only two-dimensional status, it is viable to compute the security-domain probability by Eq. (9). However, for multi-generator power systems, the calculation is complicated owing to the multi-dimensional running status. The energy function for multi-machine power systems (7) can be represented as follows:[28]

$$\begin{aligned}\mathcal{H} =& \frac{1}{2}\sum_{i=1}^{n} M_i\omega_0\Delta\omega_i^2+\sum_{i=1}^{n}P_i(\delta_{is}-\delta_i)\\&+\sum_{i=1}^{n}\sum_{j=i+1}^{n}E_iE_jB_{ij}\cos(\delta_{is}-\delta_{js})\\&-\sum_{i=1}^{n}\sum_{j=i+1}^{n}E_iE_jB_{ij}\cos(\delta_i-\delta_j),\end{aligned}\tag{10}$$

where δ_{is} and δ_{js} are respectively the balanced rotating angles for the i-th and j-th machines.

A domain where the energy function $\mathcal{H}$ is below the critical energy $\mathcal{H}_{\rm B}$ is termed the bounded fluctuation domain. The critical energy $\mathcal{H}_{\rm B}$ can be established based on the operational demands. Therefore, the security-domain probability can be transferred as

$$\boldsymbol{P}(t)=\boldsymbol{P}\{\mathcal{H}(t)<\mathcal{H}_{\rm B}\},\tag{11}$$

where $\mathcal{H}(t)$, $\mathcal{H}_{\rm B}$, and $\boldsymbol{P}\{\mathcal{H}(t)<\mathcal{H}_{\rm B}\}$ stand for the system energy at time t, the critical energy, and the possibility that $\mathcal{H}(t)$ is less than $\mathcal{H}_{\rm B}$, respectively.

4. FGN-induced theoretical analysis for power systems

In the present part, FGN-induced stochastic dynamical analysis in power systems is utilized to analytically compute the security-domain probability. First, we provide a concise overview of the integral and differential rules concerning FBM and FGN, accompanied by a sample solution of a linear system to FGN. Second, the explicit solution for the system energy is acquired based on mathematical derivation. Finally, the security-domain probability is calculated analytically according to the statistical knowledge of the system energy.

4.1. Pathwise integrals and differential rule for FBM

A number of stochastic integral definitions for the FBM have been proposed in various fields.[14–16] The pathwise integral is the simplest and most natural of these. Consider the following summation:

$$\begin{aligned}&\int_{t_0}^{t} f(X(s),s)\,{\rm d}B^H(s)\\&=\lim_{n\to\infty}\sum_{i=1}^{n} f(X(t_i'),t_i')[B^H(t_i)-B^H(t_{i-1})],\\&t_i=i\Delta t,\quad \Delta t=\frac{(t-t_0)}{n},\end{aligned}\tag{12}$$

where $t_{i-1}\le t_i'\le t_i$; $f(X(t),t)$ is a function of the random process $X(t)$ and time t. There are three different types of pathwise integrals according to $t_i'=(t_{i-1}+t_i)/2$, $t_i'=t_{i-1}$ or $t_i'=t_i$.

The first is called the symmetric integral, which is defined as

$$\begin{aligned}&\int_{t_0}^{t} f(X(s),s)\,{\rm d}^{\circ}B^H(s)\\&=\lim_{n\to\infty}\sum_{i=1}^{n} f\left(X\left(\frac{t_{i-1}+t_i}{2}\right),\frac{t_{i-1}+t_i}{2}\right)[B^H(t_i)-B^H(t_{i-1})],\\&t_i=i\Delta t,\quad \Delta t=\frac{(t-t_0)}{n},\end{aligned}\tag{13}$$

where $\int\cdot\,{\rm d}^{\circ}B^H(s)$ denotes the symmetric integral. The second is called the forward integral, which is defined as

$$\begin{aligned}&\int_{t_0}^{t} f(X(s),s)\,{\rm d}^{-}B^H(s)\\&=\lim_{n\to\infty}\sum_{i=1}^{n} f(X(t_{i-1}),t_{i-1})[B^H(t_i)-B^H(t_{i-1})],\\&t_i=i\Delta t,\quad \Delta t=\frac{(t-t_0)}{n},\end{aligned}\tag{14}$$

where $\int\cdot\,{\rm d}^{-}B^H(s)$ denotes the forward integral. The third is called the backward integral, which is defined as

$$\begin{aligned}&\int_{t_0}^{t} f(X(s),s)\,{\rm d}^{+}B^H(s)\\&=\lim_{n\to\infty}\sum_{i=1}^{n} f(X(t_i),t_i)[B^H(t_i)-B^H(t_{i-1})],\\&t_i=i\Delta t,\quad \Delta t=\frac{(t-t_0)}{n},\end{aligned}\tag{15}$$

where $\int\cdot\,{\rm d}^{\circ}B^H(s)$ denotes the backward integral.

For $H=1/2$, equation (13) is exactly the Stratonovich integral, and equation (14) reduces to the Itô integral. In practical and theoretical studies, the backward integral is rarely used, while the symmetric integral and the forward integral are widely used. If an SDE is set up, the appropriate stochastic integral type must be selected. For example, the following SDE

$${\rm d}X(t)=\alpha(X(t),t)\,{\rm d}t+\beta(X(t),t)\,{\rm d}^{-}B^H(t)\tag{16}$$

is associated with the path-forward path integral. Consequently, the fractional forward processes are used to describe the stochastic process $X(t)$ governed by Eq. (16). In this paper, the path-symmetric integral and forward-integral type SDEs are used. The first is used for the modeling of the physical

equation and is then transformed into the second one. Following the definitions of the path-symmetric integral (13) and the path-forward integral (14), the difference between the two types of differentials can be simplified in the following way:

$$\begin{aligned}&\beta(X(t),t)\mathrm{d}^{\circ}B^H(t)-\beta(X(t),t)\mathrm{d}^{-}B^H(t)\\&=\begin{cases}\frac{1}{2}\frac{\partial}{\partial x}\beta(X(t),t)\mathrm{d}t, & H=1/2,\\ 0, & H>1/2.\end{cases}\end{aligned}\tag{17}$$

This means that when $H>1/2$, the forward integral and the symmetric integral are equivalent. Thus, equation (16) is equivalent to the following SDE

$$\mathrm{d}X(t)=\alpha(X(t),t)\mathrm{d}t+\beta(X(t),t)\mathrm{d}^{\circ}B^H(t),\quad H>1/2.\tag{18}$$

Consider a function $Y(t)=f(X(t),t)$ of the fractional forward process $X(t)$ governed by Eq. (16) with Hurst index $H\in(1/2,1)$. The following differential rule has been demonstrated[14,16]

$$\mathrm{d}Y(t)=\frac{\partial f(X(t),t)}{\partial t}\mathrm{d}t+\frac{\partial f(X(t),t)}{\partial x}\mathrm{d}X(t),\quad H>1/2.\tag{19}$$

This rule can be extended to the case of multiple dimensions. For example, consider the following n-dimensional fractional forward-SDE:

$$\mathrm{d}\boldsymbol{X}(t)=\alpha(\boldsymbol{X}(t))\mathrm{d}t+\beta(\boldsymbol{X}(t))\mathrm{d}^{-}\boldsymbol{B}^H(t),\tag{20}$$

where $\boldsymbol{X}=[X_1,X_2,\ldots,X_n]^{\mathrm{T}},\alpha(\boldsymbol{X}(t))$ is an $n\times 1$ vector, $\beta(\boldsymbol{X}(t))$ is an $n\times m$ matrix, and $\boldsymbol{B}^H(t)=[B_1^{H_1}(t),\ldots,B_m^{H_m}(t)]^{\mathrm{T}}$ is a vector of m independent unit FBMs with Hurst indexes $1/2<H_1,H_2,\ldots,H_m<1$. The fractional forward-SDE for $\boldsymbol{Y}(t)=f(\boldsymbol{X}(t))$ is

$$\begin{aligned}&\mathrm{d}Y(t)=f_x^{\mathrm{T}}\alpha(\boldsymbol{X}(t))\mathrm{d}t+f_x^{\mathrm{T}}\beta(\boldsymbol{X}(t))\mathrm{d}^{-}\boldsymbol{B}^H(t),\\&1/2<H_1,H_2,\ldots,H_m<1,\end{aligned}\tag{21}$$

where $f_x=[\partial f/\partial x_1,\ldots,\partial f/\partial x_n]^{\mathrm{T}}$.

4.2. Sample solution of linear SDE with FBM

Considering the following n-dimensional linear SDEs

$$\mathrm{d}\boldsymbol{X}(t)=\boldsymbol{M}\boldsymbol{X}(t)\mathrm{d}t+\boldsymbol{Q}^{-}\mathrm{d}\boldsymbol{B}^H(t),\quad \boldsymbol{X}(0)=\boldsymbol{X}_0,\tag{22}$$

where $\boldsymbol{X}(t)=[X_1(t),X_2(t),\ldots,X_n(t)]^{\mathrm{T}}$ is an $n\times 1$ vector random process; $\boldsymbol{B}^H(t)=[B_1^{H_1}(t),\ldots,B_m^{H_m}(t)]^{\mathrm{T}}$ is an $m\times 1$ vector of independent unit FBMs with Hurst indexes $1/2<H_1,H_2,\ldots,H_m<1$; $\boldsymbol{M}$ is an $n\times n$ constant coefficient matrix; $\boldsymbol{Q}$ is an $n\times m$ constant coefficient matrix modulating the excitation intensities of FBMs $\boldsymbol{B}^H(t)$. Considering function $\mathrm{e}^{-\boldsymbol{M}t}\boldsymbol{X}(t)$ and using the differential rule, we can get

$$\mathrm{d}(\mathrm{e}^{-\boldsymbol{M}t}\boldsymbol{X}(t))=-\boldsymbol{M}\mathrm{e}^{-\boldsymbol{M}t}\boldsymbol{X}(t)\mathrm{d}t+\mathrm{e}^{-\boldsymbol{M}t}\mathrm{d}\boldsymbol{X}(t),\tag{23}$$

where $\mathrm{e}^{-\boldsymbol{M}t}$ is an exponent matrix. Upon substituting the expression (22) into Eq. (23) and then completing the integration on both sides of Eq. (23), the following sample solution for Eq. (22) is obtained

$$\boldsymbol{X}(t)=\mathrm{e}^{\boldsymbol{M}t}\boldsymbol{X}_0+\int_0^t\mathrm{e}^{\boldsymbol{M}(t-s)}\boldsymbol{Q}\mathrm{d}^{-}\boldsymbol{B}^H(s).\tag{24}$$

In the presence of positive damping, the initial term $\mathrm{e}^{\boldsymbol{M}t}\boldsymbol{X}_0$ in Eq. (24) undergoes decay, approaching a state of vanishing as the temporal domain extends to an infinite extent. The secondary term approaches a state of stationarity following an infinite temporal span. Consequently, the solution of the stationary sample of the SDE (22) is as follows:

$$\boldsymbol{X}(t)=\int_{-\infty}^t\mathrm{e}^{\boldsymbol{M}(t-s)}\boldsymbol{Q}\mathrm{d}^{-}\boldsymbol{B}^H(s).\tag{25}$$

4.3. Simplifying model of system energy under FGN excitation

In reality, the magnitude of the random disturbance or excitation is relatively small; therefore, it is reasonable to linearize. The linearized model of system (7) at its equilibrium point is derived as

$$\begin{cases}\mathrm{d}\Delta\delta_i=\omega_0\Delta\omega_i\mathrm{d}t, & i=1,2,\ldots,n-1,\\ M_i\mathrm{d}\Delta\omega_i=-\sum_{j=1,j\neq i}^{n}C_{ij}(\Delta\delta_i-\Delta\delta_j)\mathrm{d}t\\ \qquad\qquad -D_i\Delta\omega_i\mathrm{d}t+\sigma_i\mathrm{d}B_i^{H_i}(t),\end{cases}\tag{26}$$

where $\Delta\delta_i=\delta_i-\delta_n$, $\Delta\delta_n=0$, δ_n is the rotor angle of the n-th machine and $C_{ij}=E_iE_jB_{ij}\cos(\delta_{is}-\delta_{js})$.

The linearized model of function (8) at its equilibrium point is represented as

$$\mathcal{H}=\frac{1}{2}\sum_{i=1}^{n}M_i\omega_0\Delta\omega_i^2+\frac{1}{2}\sum_{i=1}^{n}\sum_{j=i+1}^{n}C_{ij}(\Delta\delta_i-\Delta\delta_j)^2.\tag{27}$$

It can be seen that Eq. (27) is a quadratic type. Through the similar matrix $\boldsymbol{C}$, the power systems (26) are transformed into

$$\mathrm{d}\boldsymbol{Y}=\boldsymbol{A}\boldsymbol{Y}\mathrm{d}t+\boldsymbol{G}\mathrm{d}\boldsymbol{B}^H(t).\tag{28}$$

The function equation (27) can be converted into the normal quadratic type

$$\mathcal{H}=\boldsymbol{Y}^{\mathrm{T}}\boldsymbol{Y}=y_1^2+\ldots+y_i^2+\ldots+y_{2n-1}^2,\tag{29}$$

where $\boldsymbol{Y}=\boldsymbol{C}\boldsymbol{X}=(y_1,\ldots,y_i,\ldots,y_{2n-1})^{\mathrm{T}}$, $\boldsymbol{X}=(\Delta\delta_1,\ldots,\Delta\delta_{n-1},\Delta\omega_1,\ldots,\Delta\omega_n)^{\mathrm{T}}$, and $\boldsymbol{C}$ is a linear transformation matrix of order $(2n-1)$.

4.4. Analytical solution for the security-domain probability

According to the pathwise integrals and differential rules w.r.t. FBM (see Subsection 4.1) and Eq. (24), the sample solution for Eq. (28) is obtained as follows:

$$\boldsymbol{Y}(t) = \mathrm{e}^{\boldsymbol{A}t}\boldsymbol{Y}_0 + \int_0^t \mathrm{e}^{\boldsymbol{A}(t-s)}\boldsymbol{G}\mathrm{d}^{-}\boldsymbol{B}^H(s). \tag{30}$$

The mean and variance of $\boldsymbol{Y}(t)$ are yielded as

$$\begin{cases} \boldsymbol{\mu}_{\boldsymbol{Y}} = \mathbb{E}\left[\mathrm{e}^{\boldsymbol{A}t}\boldsymbol{Y}_0 + \int_0^t \mathrm{e}^{\boldsymbol{A}(t-s)}\boldsymbol{G}\mathrm{d}^{-}\boldsymbol{B}^H(s)\right] = \mathbb{E}[\boldsymbol{Y}_0]\,\mathrm{e}^{\boldsymbol{A}t}, \\ \boldsymbol{\Sigma}_{\boldsymbol{Y}} = \mathbb{E}\left[\left(\mathrm{e}^{\boldsymbol{A}t}\boldsymbol{Y}_0 + \int_0^t \mathrm{e}^{\boldsymbol{A}(t-s)}\boldsymbol{G}\mathrm{d}^{-}\boldsymbol{B}^H(s) - \mathbb{E}[\boldsymbol{Y}(t)]\right)^2\right] \\ \quad = H(2H-1)\int_0^t\int_0^t \mathrm{e}^{\boldsymbol{A}(t-u)} \\ \quad\quad \times \boldsymbol{G}\boldsymbol{G}^{\mathrm{T}}\mathrm{e}^{\boldsymbol{A}(t-v)}|u-v|^{2H-2}\mathrm{d}u\mathrm{d}v, \end{cases} \tag{31}$$

where $1/2 < H < 1$, $\boldsymbol{\mu}_{\boldsymbol{Y}}$ and $\boldsymbol{\Sigma}_{\boldsymbol{Y}}$ are respectively the mean and variance.[16]

It is not difficult to find that $\boldsymbol{Y}(t)$ follows the multivariate normal distribution $N(\boldsymbol{\mu}_{\boldsymbol{Y}}, \boldsymbol{\Sigma}_{\boldsymbol{Y}})$. The Wishart distribution is then the probability distribution of the random variable $\mathcal{H} = \boldsymbol{Y}^{\mathrm{T}}\boldsymbol{Y}$. The probability density function (PDF) of the system energy $\mathcal{H}$ (29) can be obtained

$$f(\mathcal{H},t) = \frac{|\mathcal{H}|^{(2n-3)/2}\exp\left(-\frac{1}{2}\mathrm{tr}\left(\boldsymbol{\Sigma}_Y^{-1}\mathcal{H}\right)\right)}{2^{(2n-1)/2}|\boldsymbol{\Sigma}_Y|^{(2n-1)/2}\Gamma\left(\frac{2n-1}{2}\right)}, \tag{32}$$

where $|\boldsymbol{\Sigma}_Y|$ is the determinant of $\boldsymbol{\Sigma}_Y$ and $\Gamma(\cdot)$ is the gamma function defined as

$$\Gamma\left(\frac{2n-1}{2}\right) = \int_0^{\infty} t^{\frac{2n-3}{2}}\mathrm{e}^{-t}\mathrm{d}t. \tag{33}$$

The PDF (32) is an essential feature for the system energy under FGN excitation. The security-domain probability (11) is indeed the integral of the PDF. Integrating Eq. (32), we have

$$\begin{aligned} \boldsymbol{P}\{\mathcal{H}(t) < \mathcal{H}_{\mathrm{B}}\} &= \int_{-\infty}^{\mathcal{H}_{\mathrm{B}}} p(\mathcal{H},t)\mathrm{d}\mathcal{H} \\ &= \int_0^{\mathcal{H}_{\mathrm{B}}} \frac{|\mathcal{H}|^{(2n-3)/2}\exp\left(-\frac{1}{2}\mathrm{tr}\left(\boldsymbol{\Sigma}_Y^{-1}\mathcal{H}\right)\right)}{2^{(2n-1)/2}|\boldsymbol{\Sigma}_Y|^{(2n-1)/2}\Gamma\left(\frac{2n-1}{2}\right)}\mathrm{d}\mathcal{H}. \end{aligned} \tag{34}$$

5. Case studies

Next, an example is used to analyze the precision and workpiece ratio of the analytical approach.

5.1. Monte Carlo method

The Monte Carlo approach will be employed to make a comparison with the analytical method. In the application of the Monte Carlo approach, determining appropriate iteration numbers and time steps is of utmost importance. Although more reliable results can be achieved by increasing the number of repetitions and reducing the time increment, this inevitably leads to a longer computational time. During the simulation process, the time step and iteration number for the Monte Carlo method can be set to 0.0001 s and 6000, respectively. The procedure for calculating the security-domain probability based on the Monte Carlo approach is illustrated in Fig. 6.

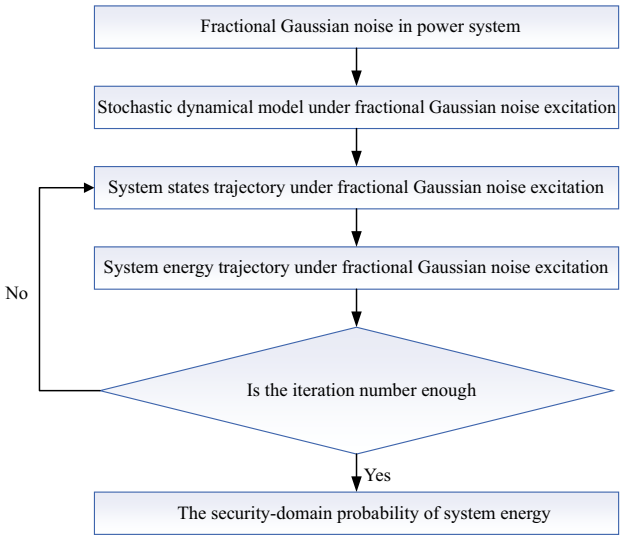

Fig. 6. Procedure to calculate security-domain probability using the Monte Carlo method.

5.2. The 4-generator 2-area power systems

The 4-generator 2-area power system will be employed as the example to be simulated, as seen in Fig. 7. These parameters can be accessed in Ref. [28]. The FGN can be described as the random perturbation of the bus load power with long-range dependence. The model of the 4-generator 2-area power system can be represented as Eq. (26).

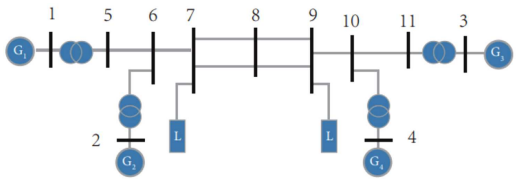

Fig. 7. The 4-generator 2-area power systems.

The time domain simulations of Eqs. (7) and (12) are carried out by using the Monte Carlo method, with the calculated state inserted into Eqs. (10) and (13). In contrast, the analytical solution for the system energy is derived through Eq. (14). This process enables the determination of the change curve of system energy with respect to time. As illustrated in Figs. 8(a)–8(c), the system energy change curves result from multiple time domain simulations with different methods. It should be noted that, within the parameters of this simulation, the critical potential energy of the original systems is estimated to be 2.2, *i.e.* $\mathcal{H}_{\mathrm{B}} = 2.2$. In other words, the systems are considered to be unstable when the energy exceeds 2.2. As shown

in Fig. 8, we can clearly observe that there is no significant difference in the trends of the energy $\mathcal{H}$ of the original system, the $\mathcal{H}$ of the linearized system, and the $\mathcal{H}$ of the obtained analytical solution. Consequently, the numerical simulations will stop once the system energy $\mathcal{H}$ surpasses 2.2, as illustrated by the red thick line.

Based on multiple numerical simulations, the probability of falling within a certain energy interval is counted at a determined moment, which is considered as the PDFs of the original systems by Monte Carlo simulation. Figures 9(a)–9(c) show the PDFs of the system energy by Eqs. (10), (27), and (29) from different times under Hurst index $H = H_1 = H_2 = H_3 = H_4 = 0.55$. More detailed results with different Hurst indexes H ($H = 0.75$ and $H = 0.95$) can be found in Fig. 10 and Fig. 11. It is noted that at fixed times $t = 3$ s, 5 s, and 7 s with different Hurst index H, the analytical solutions agree well with the PDFs of the original system energy and the linearized model of system energy. Meanwhile, as shown in Fig. 12, by comparing the PDFs of the system energy at different times with different Hurst indexes H, we can find that although the mean value of the system energy decreases when H approaches 1 from 0.5, the probability of the tail increases.

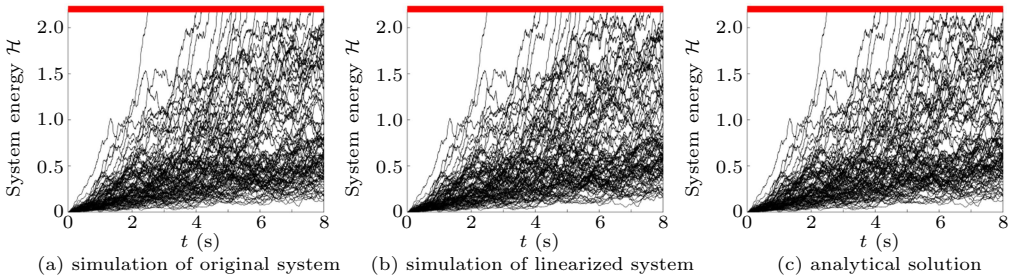

Fig. 8. Energy curve based on time domain simulation under $H_1 = H_2 = H_3 = H_4 = 0.75$.

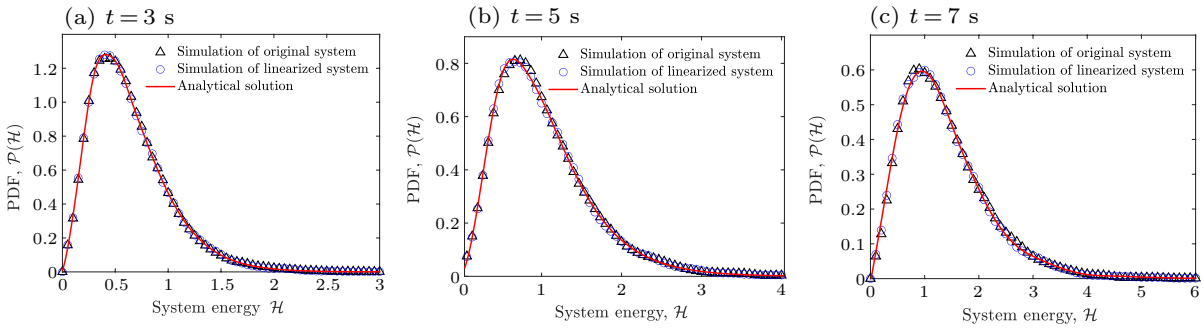

Fig. 9. The comparison with PDF of system energy from different times under $H_1 = H_2 = H_3 = H_4 = 0.55$.

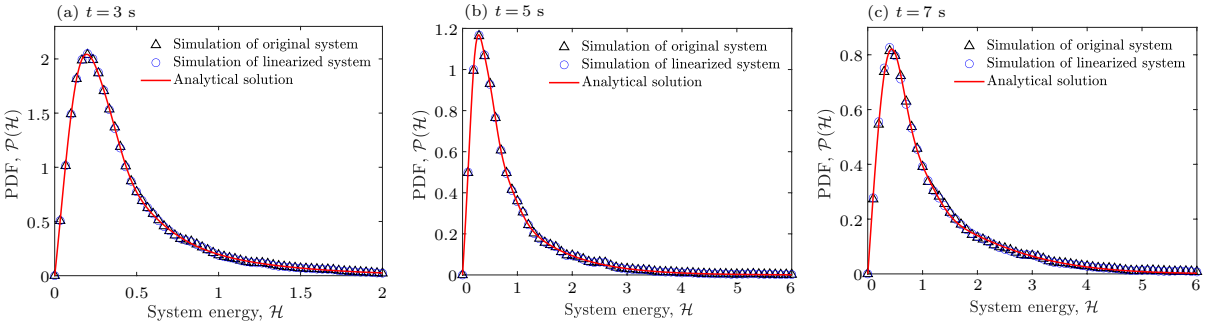

Fig. 10. The comparison with PDF of system energy from different times under $H_1 = H_2 = H_3 = H_4 = 0.75$.

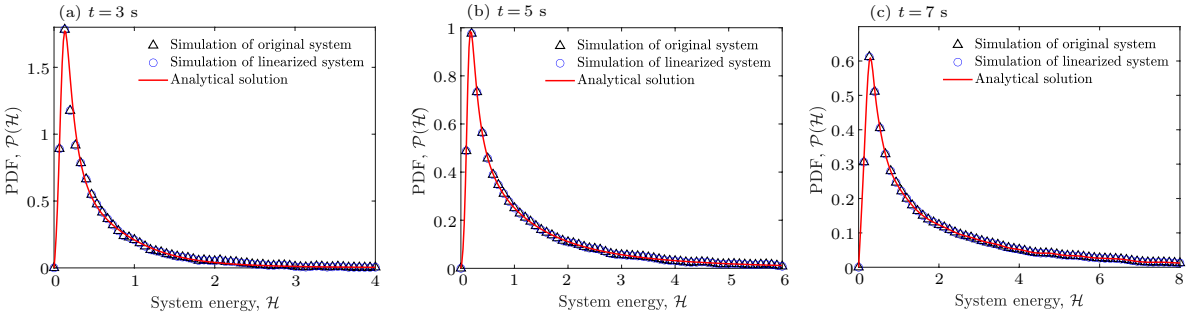

Fig. 11. The comparison with PDF of systems energy from different times under $H_1 = H_2 = H_3 = H_4 = 0.95$.

Furthermore, we can derive the security-domain probability in accordance with the PDFs, which is considered a reliable indicator to estimate the effect of FGN excitation on power system characteristics. In the simulation example, the security-domain probability is studied using the analytical method and the Monte Carlo method. The security-domain probability is calculated for different Hurst indexes, intensities of FGN, damping factors and critical energy, as seen from Fig. 13. Obviously, all findings from the analytical method are extremely close to the Monte Carlo approach, indicating that the analytical approach has high accuracy. Figure 13(a) plots the security-domain probability under different Hurst indexes (Case 1: $H = H_1 = H_2 = H_3 = H_4 = 0.55$, Case 2: $H = H_1 = H_2 = H_3 = H_4 = 0.75$, Case 3: $H = H_1 = H_2 = H_3 = H_4 = 0.95$). Figure 13(b) shows the security-domain probability at different strengths of FGN (Case 1: $\sigma_1 = 0.03$, $\sigma_2 = 0.04$, $\sigma_3 = 0.05Z$, $\sigma_4 = 0.06$; Case 2: $\sigma_1 = 0.04$, $\sigma_2 = 0.05$, $\sigma_3 = 0.06$, $\sigma_4 = 0.07$; Case 3: $\sigma_1 = 0.06$, $\sigma_2 = 0.07$, $\sigma_3 = 0.08$, $\sigma_4 = 0.09$) when the Hurst index is $H = H_1 = H_2 = H_3 = H_4 = 0.75$. Figure 13(c) displays the security-domain probability at damping factors (Case 1: $D_1 = 0.60$, $D_2 = 0.65$, $D_3 = 0.70$, $D_4 = 0.75$; Case 2: $D_1 = 0.50$, $D_2 = 0.55$, $D_3 = 0.60$, $D_4 = 0.65$; Case 3: $D_1 = 0.40$, $D_2 = 0.45$, $D_3 = 0.50$, $D_4 = 0.55$) with a fixed Hurst index $H = 0.75$. Figure 13(d) shows the security-domain probability at different critical energies (Case 1: $\mathcal{H}_B = 8$, Case 2: $\mathcal{H}_B = 6$, Case 3: $\mathcal{H}_B = 4$) when the Hurst index is $H = H_1 = H_2 = H_3 = H_4 = 0.75$. From Fig. 13, the security-domain probability increases with the increase of the Hurst index, damping factor and critical energy, and with the decrease of FGN strength, respectively. Enhancing system damping, mitigating FGN excitation and improving the tolerance of the systems with respect to stochastic noise will contribute to the regulation and operation of power systems under FGN excitation.

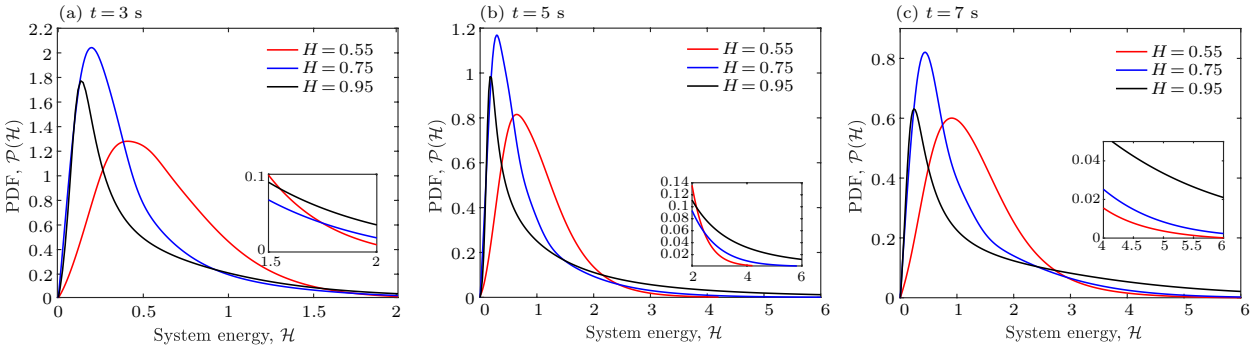

Fig. 12. The comparison with PDF of system energy from different times under $H_1 = H_2 = H_3 = H_4 = 0.95$.

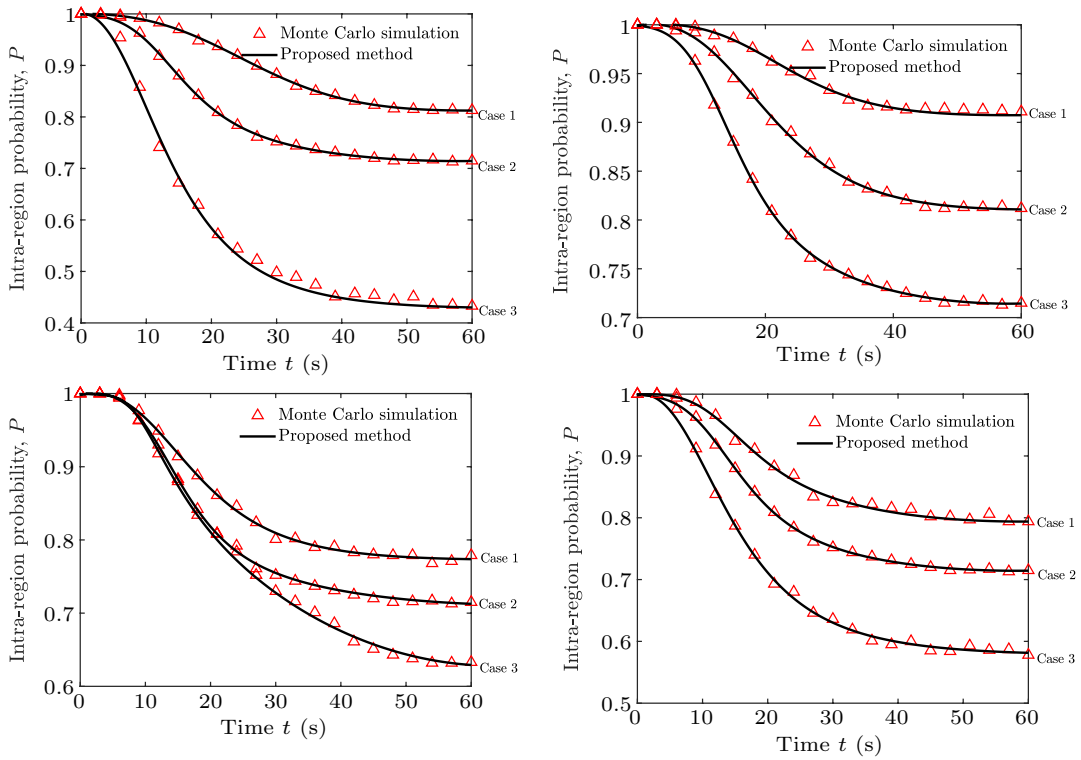

Fig. 13. The security-domain probability under several conditions with different Hurst indexes, strengths of FGN excitation, damping factors and critical energy.

6. Conclusion

Due to the convenience of new energy and chargeable vehicles, the random noises in the power systems are of great concern. In this article, an advanced analytical method is developed to evaluate the dynamical effects with FGN excitation on power systems. Firstly, it is reasonable, effective and necessary to introduce FGN into power systems to describe the randomness with time-correlation and probability characteristics. The security-domain probability is employed to evaluate the dynamical effects of FGN excitation. Secondly, according to pathwise integrals and the differential rule w.r.t. FBM, the analytical method is developed to evaluate the dynamical influences of FGN excitation on power systems. To verify the effectiveness of the proposed method, the Monte Carlo solution of the original systems is used as the reference solution. Finally, some suggestions are given to increase the system damping, mitigate external random disturbances and increase the tolerance of the systems with random disturbances to promote the dynamical characteristics of the power systems. In practical implementation, the damping value of power systems should be appropriately increased. Through measures of system correction, filtering processing and setting a reasonable controller, the tolerance of the systems to stochastic disturbance will be improved.

The proposed method has several advantages, including high efficiency and a clear mechanism, which meet the requirements of more intelligent power systems. Facing the access of large-scale renewable energy and active load, the research in this paper has certain theoretical significance and practical application value. Using much more detailed power grid models and multiplicative FGN excitation will be the focus of the next research work.

Acknowledgements

Project supported by the National Natural Science Foundation of China (Grant No. 12362005), the Ningxia Higher Education First-class Discipline Construction Funding Project (Grant No. NXYLXK2017B09), the Key Project of Natural Science Foundation of Ningxia Hui Autonomous Region, China (Grant No. 2024AAC02033), Guangdong Basic and Applied Basic Research Foundation (Grant No. 2024A1515012164), the Foundation of MOE Key Laboratory for Complexity Science in Aerospace, Northwestern Polytechnical University (Grant No. CSA-ZD202401), and the Fundamental Research Funds for the Central Universities.

References

[1] Yang C, Sun W, Han D and Yin X 2022 *Front. Energy* **10** 967220
[2] Wang L Q, Liu H Q, Wang Q, Cong Y and Zheng X X 2024 *J. Phys.: Conf. Ser.* **2874** 012012
[3] Gu Y Z and Xie L 2017 *IEEE Trans. Power Syst.* **32** 2520498
[4] Wan Y and Ji Z H 2022 *IEEE Trans. Power Syst.* **38** 3205953
[5] Ju P, Li H Y, Gan C, Liu Y, Yu Y P and Liu Y L 2018 *IEEE Trans. Power Syst.* **33** 2720687
[6] Odun-Ayo T and Crow L M 2013 *Int. T. Electr. Energy* **23** 646
[7] Yuan B, Zhou M, Li G, Zhang X P 2014 *IEEE Trans. Power Syst.* **30** 2353014
[8] Wang K and Crow M L 2012 *IEEE Trans. Power Syst.* **28** 2232317
[9] Ghanavati G, Hines P D and Lakoba T I 2015 *IEEE Trans. Power Syst.* **31** 2412115
[10] Ju P, Li H Y, Pan X P, Gan C, Liu Y and Liu Y L 2018 *IEEE Trans. Power Syst.* **33** 2777783
[11] Li H F and Ma S J 2023 *Mathematics* **11** 2854
[12] Vyushin D I and Kushner P J 2009 *J. Climate* **22** 2528
[13] Wang Z, Zhu J J and Liu X B 2025 *Physica D* **482** 134919
[14] Biagini F, Hu Y, Øksendal B and Zhang T 2008 *Stochastic Calculus for Fractional Brownian Motion and Applications* (Springer Science & Business Media)
[15] Mishura Y 2008 *Stochastic Calculus for Fractional Brownian Motion and Related Processes* (Springer)
[16] Deng M L and Zhu W Q 2015 *ASME. J. Appl. Mech.* **82** 101008
[17] CPTEC 2022 *Centro de previsão de tempo e estudos climáticos El Niño e La Niña*
[18] Shah S M A, Nie Y F, Din A, Alkhazzan A and Younas B 2024 *Chin. Phys. B* **33** 110203
[19] Peng C K, Buldyrev S V, Havlin S, Simons M, Stanley H E and Goldberger A L 1994 *Phys. Rev. E* **49** 1685
[20] de Oliveira Santos M, Stosic T and Stosic B D 2012 *Physica A* **391** 1546
[21] Zhu R, Yuan W, Fei Q, Chen Q, Fan G, Marchesiello S and Anastasio D. 2025 *Eng. Struct.* **323** 119238
[22] Wang F, Shieh S J, Havlin S and Stanley H E 2009 *Phys. Rev. E* **79** 056109
[23] dos Anjos P S, da Silva A S A, Stosic B and Stosic T 2015 *Physica A* **424** 90
[24] Li Z K and Li D X 2023 *Chin. Phys. B* **32** 010203
[25] Mandelbrot B B and Van Ness J W 1968 *SIAM Rev.* **10** 422
[26] Eftekharnejad S, Vittal V, Heydt G T, Keel B and Loehr J 2013 *IEEE Trans. Sustain. Energy* **4** 2259602
[27] Zhu R, Jiang D, Marchesiello S, Anastasio D, Zhang D H and Fei Q G2023 *AIAA J.* **61** 062816
[28] Kundur P S 2022 *Power System Stability and Control* (McGraw-Hill Education)
[29] Huang X T, Li D S and Wang L H 2011 *J. Math. Anal. Appl.* **376** 443
[30] Jiang F, Shen Y and Wu F 2011 *Stoch. Anal. Appl.* **29** 216
[31] Liu H K, Lin T Y and Tsai Y L 2021 *Taiwan J. Math.* **25** 200803
[32] Madan D B 2017 *Quant. Financ.* **17** 497